



Spatio-Temporal Variability of Tidal Velocities in the Rivers of the Indian Sundarban Delta: A Hydrodynamic Modelling Approach

Koushik Bhui¹ · Sugata Hazra¹ · Tuhin Bhadra^{1,2} · Vengatesan Venugopal³

Received: 24 June 2020 / Accepted: 4 November 2021 / Published online: 12 January 2022
© The Institution of Engineers (India) 2021

Abstract This study investigates the spatio-temporal variability of tidal velocities in the Sundarban River System. The industry standard numerical tool MIKE 21 Flow Model was applied to simulate tidal velocities in the river system. Bathymetry data from GEBCO (<https://www.gebco.net/>) and surveyed bathymetry were used in model construction. The tidal velocities were measured using Acoustic Doppler Current Profiler at two tidal channels, namely Chaltabani Khal in the south and Durgaduani Creek in the north. The simulated tidal velocities were compared with the observed tidal velocities at two different locations at two different times to calibrate and validate the model. The validated model identified 11 high-velocity sites within the Sundarbans, where flow velocity of up to 2.46 m/s was observed for the study period. The highest tidal velocity along with the higher tidal ranges was found during the March equinox (March/April), whereas the lowest velocity along with the lower tidal ranges was observed during the summer solstice (July/August). The results showed that the velocities within the narrow channels were stronger compared to those in the wider channels. The simulations revealed that about 53% of tidal velocities were more than 1 m/s throughout a day in a particular site on the Bidyadhari River. A variation of tidal velocities from 0.5 to 1.0 m/s was also observed for other areas for a

higher period during a day. This study also found that the shorter flood tide period caused stronger flood tidal velocity than the ebb-tidal velocity. Seven possible deployment locations for harnessing tidal energy in the Sundarbans delta were identified by the model in this study. It is expected that the study, the first of its kind in this region, will be useful in developing and planning for coastal resilience and sustainable development in a delta vulnerable to climate change and sea-level rise.

Keywords Indian Sundarbans · Hydrodynamic modelling · MIKE21 · ADCP · Tidal velocity · Spatio-temporal variability

Introduction

The world's largest mangrove forest, the Sundarbans, is situated in the world's most extensive deltaic plain, formed by the fluvio-marine sedimentation of the distributaries of the Ganges and the Brahmaputra River at their confluence in the Bay of Bengal (BoB) [1–3]. The Head of BoB, where the Sundarbans mangrove forest exists, has a shallow bathymetry, low-lying topography, funnel-shaped coastline, and high tidal range that make the Sundarbans vulnerable to floods, storm surges, inundation, and coastal erosion [4]. Along with the mangrove forest, the delta is shared by two neighbouring countries, India and Bangladesh. In the Indian part, seven estuaries exist from the west to the east; they are Hugli, Muriganga, Saptamukhi, Thakuran, Matla, Gosaba, and Harinbhanga, as shown in Fig. 1. The field measurements and numerical prediction of velocity patterns of the tidal rivers help to assess the tidal effects, hydrodynamic (HD) activities, morphological behaviour, erosion–accretion processes, sedimentation

✉ Koushik Bhui
iamkoushikbhui@gmail.com

¹ School of Oceanographic Studies, Jadavpur University, Kolkata, India

² Department of Geography, Adamas University, Kolkata, India

³ Institute of Energy System, School of Engineering, University of Edinburgh, Edinburgh, UK

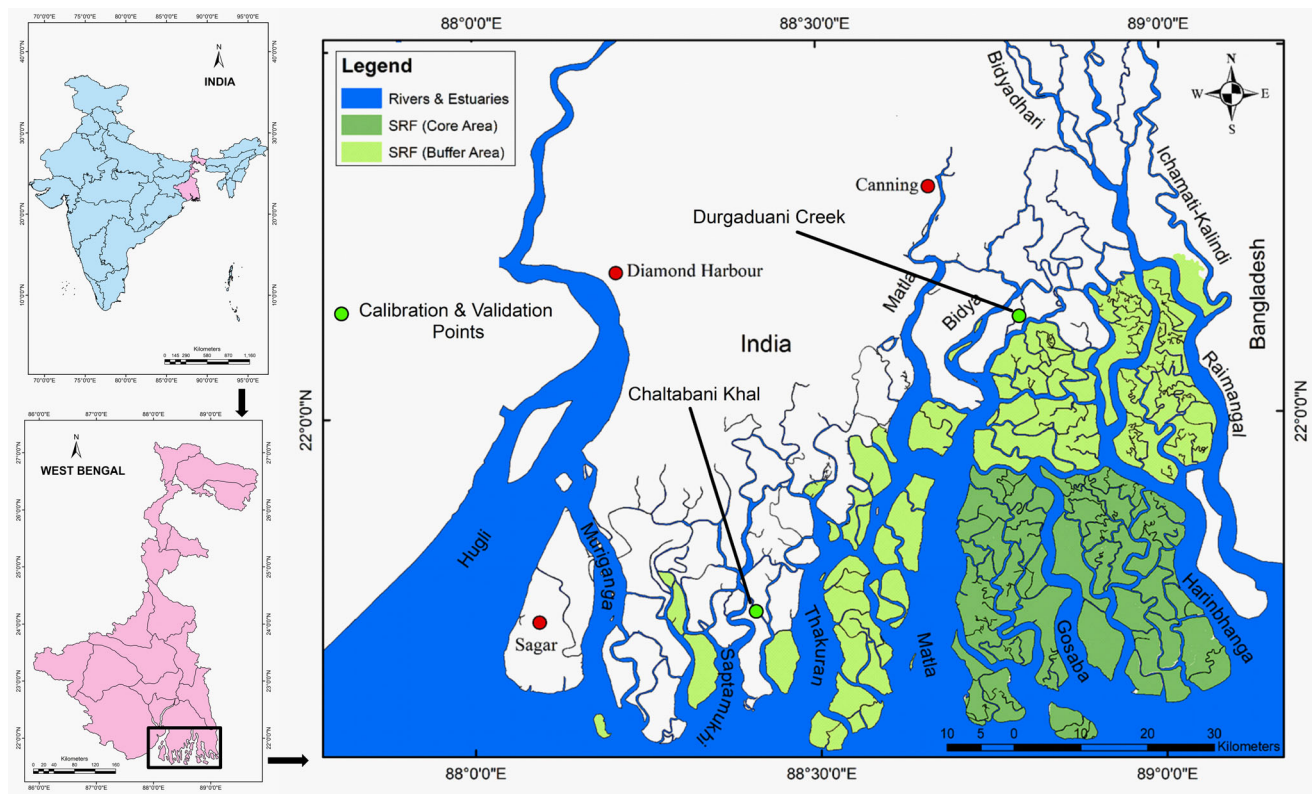


Fig. 1 Sundarbans Estuarine River System, India

process, water quality, turbulent diffusion, and navigation system. Besides, for constructing embankments, erosion protection plans, jetties, island management plans, and even for the generation of tidal energy from the high-velocity fields, assessment, monitoring, and prediction of tidal velocities are the need of the hour, and hence, the primary objective of this study.

Several numerical modelling studies concerning tidal behaviour have been conducted globally in the estuarine environment and coastal regions. A three-dimensional (3D) mathematical model was applied in the Jakarta Bay, Indonesia by Radjawane and Riandini [5] to simulate the tidal velocities and cohesive sediment transport, analysing the effect of tidal velocities and river discharge. Dabrowski et al. [6] simulated tidal velocities and tidal elevation using two-dimensional (2D) and 3D numerical models to analyse HD circulation patterns in the Irish Sea. Kumar & Balaji [7] simulated tidal velocities for estimating tidal current energy along the Gulf of Khambhat using the 3D numerical model Delft3D-FLOW. A 2D HD numerical model was constructed using Telemac system by Blunden and Bahaj [8] to evaluate the tidal stream energy resources at Portland Bill in the UK, and the result of the model was used to produce sufficient power from a turbine. Balachandran et al. [9] constructed a 2D HD model using Hydrodyn-FLOSOFT to simulate the propagation of tidal circulation

for pollutant dispersion in the Cochin estuary. Babu et al. [10] used the MIKE 21 HD model to simulate tide-driven currents and residual eddies in the Gulf of Kachchh for three different periods (NE monsoon, Pre-monsoon, and SE monsoon). Rahman and Venugopal [11] used Telemac3D and Delft3D models to assess tidal resources in the Pentland Firth in Scotland, United Kingdom, and the results indicated that both Telemac3D and Delft3D models are able to produce excellent comparison against measured data. Telemac3D was also used to model tidal turbines in a tidal channel by Rahman et al. [12]. Kumar et al. [13] studied storm surges of Andaman Island in the Indian Ocean, simulating a 2D HD model using MIKE21 from the Danish Hydraulic Institute (DHI).

Due to the scarcity of observational data, very few studies on tidal dynamics have been carried out in the Indian Sundarbans Delta (ISD). Murty and Henry [14] used a finite difference numerical model in this region to produce co-tidal charts for principal tidal constituents. A 2D numerical model was formulated by Sindhu and Unnikrishnan [15] to simulate major tidal components. Bhat-tacharyya et al. [16] studied morphology and the tidal environment of the Sundarbans Estuaries. Chatterjee et al. [17] first conducted the Sundarban Estuarine Programme (SEP) to monitor the tidal variation at 30 observational stations for a short period within the Sundarban Estuarine

System (SES). Gayathri et al. [18] used the Advanced Circulation (ADCIRC) model to simulate hypothetical storm surge and inundation by ‘Aila’ cyclone of 2009 in the Sundarbans delta. To simulate tidal hydrodynamics and freshwater flow in the Ganges–Brahmaputra–Meghna (GBM) delta, Briceno et al. [19] first employed the 3D baroclinic model—Finite Volume Community Ocean Model (FVCOM), using available General Bathymetric Charts of the Oceans (GEBCO) and ETOPO bathymetry. Antony et al. [20] studied the evolution of water levels along the east coast of India and found the most significant magnitude of the highest water level above the Mean Sea Level (MSL) towards the northern part of Bay and decreased towards the south-west. Rose and Bhaskaran [21] used the ADCIRC HD model to investigate spatial and temporal variability of tides using the wavelet techniques at the head BoB and observed their nonlinear characteristics. Therefore, no previous hydrological or HD model is calibrated to investigate the variability of tidal velocities in this region and particularly coupled with on-site bathymetric observations. Therefore, the main focus of the present study is to construct an HD model to analyse the spatial and temporal variability of tidal velocities in the rivers of the ISD with in situ validation. This study also tries to identify the possible deployment locations for harnessing tidal stream energy in the Sundarbans. Based on the literature review, we believe this was the first study that used the industry approved commercial software MIKE suite for this research region; Secondly, we believe, this is the first time, a proper numerical model of the Sundarbans Delta is constructed with a finer scale resolution of the river boundaries, including hundreds of smaller creeks, and we were not able to observe such finer refinement in other works; and thirdly, there was no information available in previously published materials about the source of bathymetry for the many of the rivers and creeks, and for the current work, we commissioned bathymetry measurements for the first time, collected representative bathymetric data within key rivers within the given constraints of budget and time. The most difficult part of this work has been, however, the inclusion and representation of water depths within these rivers. Bathymetry data available in the public domain do not cover the entire region, including tidal rivers and creeks. The popular GEBCO bathymetry covers only the region of estuarine mouth to the BoB, excluding the internal waters. However, the specific contribution of this study was that it generated data on tidal currents and water level for the entire region, and in particular, we produced detailed information for two locations, Chaltabani Khal near the Matla river and Durgaduani Creek near the Gomar river close to the NW 97, and demonstrated that the model results agreed with ADCP measurements for these locations, providing that our model performed well. We may

agree the model performance remains to be validated for other locations of the delta, for which, more field measurement data are required to prove this which remained beyond the scope of this pilot study.

Data and Methodology

Field Observations

The bathymetry surveys were conducted by the School of Oceanographic Studies, Jadavpur University, India, in the internal rivers and creeks of the Sundarbans using Garmin 100 xs Aqua map series with Airmar B175 m Transducer with moving boats, from February 2016 to February 2018. The hourly tidal velocity data at the Durgaduani Creek and the Chaltabani Khal were measured using River Ray Acoustic Doppler Current Profiler (ADCP) 600 kHz instrument to calibrate and validate the HD model. The tidal velocities were measured at the Chaltabani Khal from 6th September 2017 to 8th September 2017 during spring tide for the calibration of the model, and from 25th December 2017 to 26th December 2017 during neap tide for the validation of the model. On the other hand, the velocity data were also recorded at the Durgaduani Creek from 2nd March 2017 to 17th March 2017. For Durgaduani Creek, the measuring duration was divided into two parts to calibrate and validate the numerical model.

Hydrodynamic Modelling using MIKE 21

The MIKE 21 Flow Model, an advanced computational HD modelling system based on a flexible mesh (FM) approach, was used to accomplish the present study. MIKE 21 is depth-integrated standard software developed by DHI (<https://www.mikepoweredbydhi.com/>) and used for advanced numerical modelling of hydrodynamics, sand transport, mud transport, waves, and ecological modelling within the oceanographic, coastal, and estuarine environment [22]. The HD module in MIKE 21 depends on the equation of the depth-integrated Reynolds averaged Navier–Stokes equation that implemented the assumptions of Boussinesq and hydrostatic pressure [22]. The model utilizes the conservation of mass and momentum (integrated over the depth) equations (Eqs. 1, 2 and 3) to describe the flow and water level variation within an estuary [22]. The governing equations are as follows:

The continuity equation:

$$\frac{\partial h}{\partial t} + \frac{\partial h\bar{u}}{\partial x} + \frac{\partial h\bar{v}}{\partial y} = hS \quad (1)$$

The momentum equation in the x-direction:

$$\begin{aligned} \frac{\partial h\bar{u}}{\partial t} + \frac{\partial h\bar{u}^2}{\partial x} + \frac{\partial h\bar{v}\bar{u}}{\partial y} = f\bar{v}h - gh\frac{\partial\eta}{\partial x} - \frac{h}{\rho_0}\frac{\partial p_a}{\partial x} - \frac{gh^2}{2\rho_0}\frac{\partial\rho}{\partial x} + \frac{\tau_{sx}}{\rho_0} - \frac{\tau_{bx}}{\rho_0} \\ - \frac{1}{\rho_0}\left(\frac{\partial s_{xx}}{\partial x} + \frac{\partial s_{xy}}{\partial y}\right) + \frac{\partial}{\partial x}(hT_{xx}) + \frac{\partial}{\partial y}(hT_{xy}) + hu_s S \end{aligned} \quad (2)$$

The momentum equation in the y-direction:

$$\begin{aligned} \frac{\partial h\bar{v}}{\partial t} + \frac{\partial h\bar{v}^2}{\partial y} + \frac{\partial h\bar{u}\bar{v}}{\partial x} = -f\bar{u}h - gh\frac{\partial\eta}{\partial y} - \frac{h}{\rho_0}\frac{\partial p_a}{\partial y} - \frac{gh^2}{2\rho_0}\frac{\partial\rho}{\partial y} + \frac{\tau_{sy}}{\rho_0} - \frac{\tau_{by}}{\rho_0} \\ - \frac{1}{\rho_0}\left(\frac{\partial s_{yx}}{\partial x} + \frac{\partial s_{yy}}{\partial y}\right) + \frac{\partial}{\partial x}(hT_{xy}) + \frac{\partial}{\partial y}(hT_{yy}) + hv_s S \end{aligned} \quad (3)$$

where t is time; x and y are the Cartesian coordinates; h is total depth, $h = \eta + d$; η is water surface elevation; d is the still water depth; \bar{u} and \bar{v} are the depth-averaged velocity components in x and y directions; S is the magnitude of the discharge due to point sources; f is the Coriolis parameter; g is the acceleration due to gravity; p_a is the atmospheric pressure; ρ is the density of water; ρ_0 is a ratio of water density to air density; (τ_{sx}, τ_{sy}) and (τ_{bx}, τ_{by}) are the x and y components of the surface wind and bottom stresses; s_{xx}, s_{xy}, s_{yx} and s_{yy} are components of the radiation stress tensor. T_{xx}, T_{xy}, T_{yx} and T_{yy} are the components of the effective shear stress due to turbulence and viscous effects; (u_s, v_s) is the velocity components in x and y directions for point sources; Further details of the numerical model may be found in DHI Mike 21 user manual [22]. The following steps were organized to construct the HD model of the present work:

Boundary Conditions and Water Levels

The boundary condition is an essential factor for simulating HD models as well as numerical solutions. The land–water boundary was extracted from satellite imagery as standard ESRI vector format (.shp) and converted to .xyz. Figure 2 shows six open boundaries (Open Boundary-1 in the west, Open Boundary-2 in the south, Open Boundary-3 in the east, Open Boundary-4 in the Hugli river, Open Boundary-5 in the Matla river, and Open Boundary-6 in the Raimangal river), which were used for the model domain. The hourly water level data from 1st January 2017 to 31st December 2017 along the seven open boundaries of the study domain were derived from the Global Tide Model of DHI using MIKE 21 toolbox. The monthly tide level data of 2017 were also obtained for the Chaltabani Khal, Durgaduan Creek and Gosaba River from WXTide available at www.wxtime32.com.

Mesh Generation

Constructing an unstructured mesh is very important for modelling the nearshore coastal hydrodynamics. The mesh size is smaller in the estuarine areas and the coastal land–water transition zones, while it is larger away from the coast [23]. The precision of the model simulation results is determined by the cell size, because the model will be more accurate with the smaller cell size [24]. In the present study, an unstructured finite mesh, including 35,624 triangular elements and 22,894 nodes, was formulated for the Indian Sundarbans estuarine rivers. The mesh domain used in the present analysis covered only the rivers and creeks of the Sundarbans, while the mainland was not included in the field.

Bathymetry Setup

The bathymetry of the Sundarbans was prepared using field surveyed data and the 30 arc-second resolution GEBCO dataset, available at <https://www.gebco.net>. The bathymetry surveys were done in the rivers and creeks of the Sundarbans where the bathymetry data were unavailable. In the remaining areas, the GEBCO dataset was incorporated with the appropriate corrections. The bathymetry data in scatter format were incorporated into the generated FM using the MIKE 21 HD FM module to get a high-resolution bathymetry of the Sundarbans. Figure 2 shows the detailed bathymetry of the Sundarbans along with the mesh generated for the MIKE 21 Flow Model.

Model Setup

MIKE 21 HD FM module was used in the present study to set up the model. In the calibration process, the value of bottom stresses (τ_{bx}, τ_{by}) plays an important role to obtain a precise model output as this parameter directly controls the flow velocity. The bottom stresses depend on the value of the drag coefficient which can be determined by the Manning number (M). The Manning number was tuned from the default value to obtain results to match close between the measured data and the simulated data. The Manning number used in MIKE 21 is the reciprocal value of Manning's n . The Manning numbers, 20–40 [$m^{(1/3)}/s$], are usually used in the HD models [22]. In the study of HD modelling, Hanipah et al. [25] assigned the Manning's M coefficient of 20 [$m^{(1/3)}/s$] for the mangrove-covered channels based on the findings of Dasgupta et al. [26]. In the present study, keeping the other input parameters unchanged, a number of simulations were attempted by altering Manning's value for bed resistance and by trial and error simulation. A value of Manning's constant of 20 [$m^{(1/3)}/s$] was found to produce model parameters close

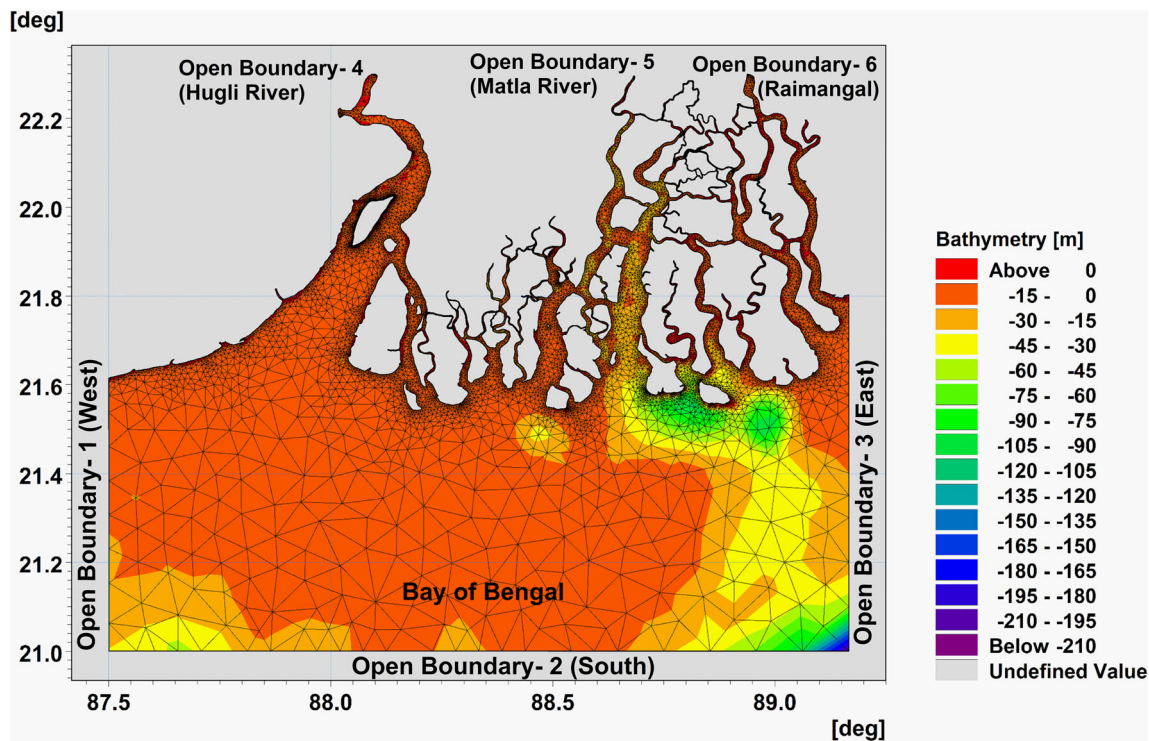


Fig. 2 MIKE 21 model domain with mesh, bathymetry map of the Sundarbans with open boundaries

to the measurement, and this value was used for further simulation. The model was simulated for each month of the year 2017. It assesses the spatial and temporal variability of water level, water depth, velocity, and current direction along and across the estuaries. In this study, the simulated velocities were extracted from the model to calibrate and validate the HD model. Figure 3 indicates the important steps of the HD model for the present research.

Model Evaluation Methods

The model was evaluated to estimate the accuracy using statistical indicators: Nash–Sutcliffe Efficiency (NSE), Percent Bias (PBIAS), RMSE–Observation Standard Deviation Ratio (RSR), and Pearson’s Coefficient of Determination (R^2). The performance of the model can be classified into four categories (i.e. Very Good, Good, Satisfactory, and Unsatisfactory) based on the indicators, as shown in Table 1 [27, 28]. The NSE, PBIAS, RSR, and R^2 were calculated using the following equations:

$$NSE = \left[1 - \frac{\sum_{i=1}^n (X_i^{obs} - X_i^{sim})^2}{\sum_{i=1}^n (X_i^{obs} - X_{obs}^{mean})^2} \right] \tag{4}$$

$$PBIAS = \frac{\sum_{i=1}^n (X_i^{obs} - X_i^{sim})^2 \times 100}{\sum_{i=1}^n X_i^{obs}} \tag{5}$$

$$RSR = \frac{RMSE}{STDEV_{obs}} = \frac{\sqrt{\sum_{i=1}^n (X_i^{obs} - X_i^{sim})^2}}{\sqrt{\sum_{i=1}^n (X_i^{obs} - X_{obs}^{mean})^2}} \tag{6}$$

$$R^2 = \left[\frac{\sum_{i=1}^n (X_i^{obs} - X_i^{sim})(X_i^{sim} - X_{sim}^{mean})}{\left\{ \sum_{i=1}^n (X_i^{obs} - X_{obs}^{mean})^2 \right\}^{0.5} \left\{ \sum_{i=1}^n (X_i^{sim} - X_{sim}^{mean})^2 \right\}^{0.5}} \right]^2 \tag{7}$$

where X_i^{obs} is the ‘i’th observed flow velocity, X_i^{sim} is the ‘i’th simulated flow velocity, X_{obs}^{mean} is the mean of the observed flow velocity, X_{sim}^{mean} is the mean simulated flow velocity, and n is the total number of observations.

Results

The performance of the MIKE 21 HD model has been reviewed in this work. The results obtained from this model are discussed, and their correlation is established to assess the spatio-temporal variability of tidal velocities in the rivers of the ISD.

MIKE 21 Model Performances

The numerical model was calibrated and validated using the measured tidal velocities at the Durgaduani Creek and the Chaltabani Khal. In order to establish model accuracy,

Fig. 3 Methodology flowchart of the present study

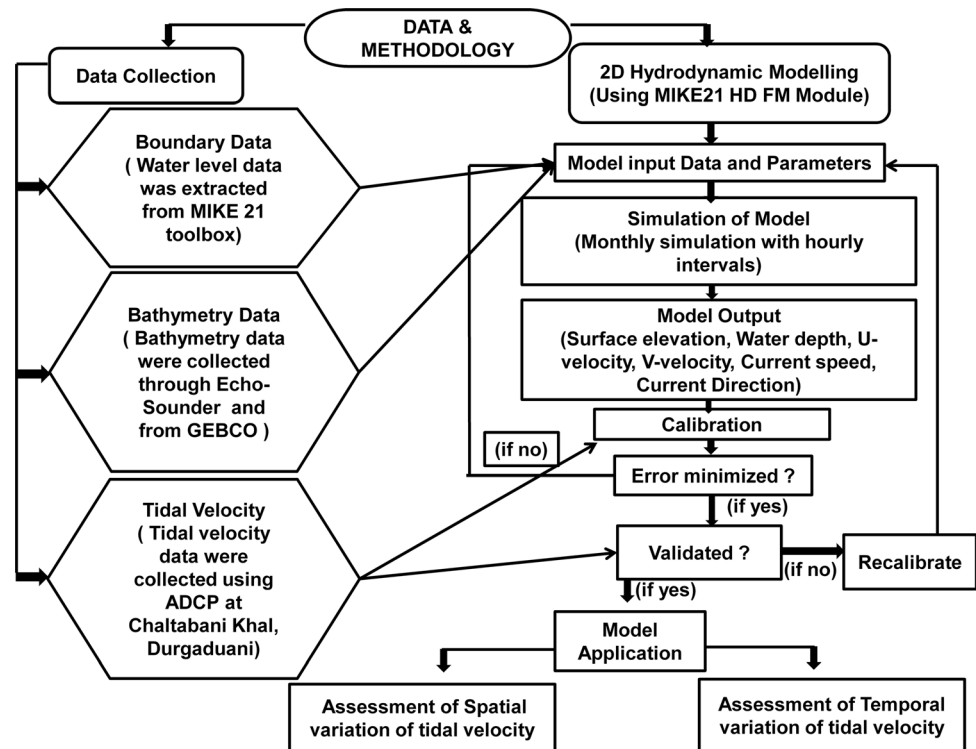


Table 1 Performance rating of HD models

| Performance | NSE | PBIAS (%) | RSR |
|----------------|-------------------------------|-------------------------------------|----------------------------------|
| Very good | $0.75 < \text{NSE} \leq 1.00$ | $\text{PBIAS} < \pm 10$ | $0.00 \leq \text{RSR} \leq 0.50$ |
| Good | $0.65 < \text{NSE} \leq 0.75$ | $\pm 10 \leq \text{PBIAS} < \pm 15$ | $0.50 < \text{RSR} \leq 0.60$ |
| Satisfactory | $0.50 < \text{NSE} \leq 0.65$ | $\pm 15 \leq \text{PBIAS} < \pm 25$ | $0.60 < \text{RSR} \leq 0.70$ |
| Unsatisfactory | $\text{NSE} \leq 0.50$ | $\text{PBIAS} \geq \pm 25$ | $\text{RSR} > 0.70$ |

the simulated data were compared with the measured data. Figure 4 shows correlation plots between the simulated and measured velocities during the calibration period (Fig. 4a and b) and the validation period (Fig. 4c and d) at the Durgaduani Creek and the Chaltabani Khal, respectively. The R^2 values are found to be more than 0.75, which indicates a good match between measurement and the model outputs. Given that the bathymetry has not been available for all the nooks and corners of the river system, this is considered a reasonable and acceptable outcome. This is evident in Fig. 5, which also depicts the comparison of time series between the simulated velocities and the measured velocities at the Durgaduani Creek and the Chaltabani Khal during the calibration period (Fig. 5a and b) and the validation period (Fig. 5c and d). The time-series graphs demonstrate a good match between the simulated velocities and the observed velocities, generally agreeing well with the variations during the flood and ebb-tidal cycles.

It will be an inappropriate method if only one goodness-of-fit measure is used to evaluate a numerical model [29]. Thus, the performance of the model in this study was assessed using some statistical indicators: (1) NSE, (2) PBIAS, (3) RMSE, and (4) R^2 during the calibration and the validation period.

The high values of R^2 (Calibration: 0.78, Validation: 0.80) (Fig. 4a and c) and NSE (Calibration: 0.73, Validation: 0.66), and the low values of RSR (Calibration: 0.52, Validation: 0.59) and PBIAS (Calibration: 3.57, Validation: 3.87), obtained for the Durgaduani Creek, indicate good model performance (refer to Tables 1 and 2 for more details). Similarly, the high values of R^2 (Calibration: 0.76, Validation: 0.83) (Fig. 4b and d) and NSE (Calibration: 0.70, Validation: 0.67), and the low values of RSR (Calibration: 0.55, Validation: 0.58) and PBIAS (Calibration: 4.49, Validation: 2.54), estimated for the Chaltabani Khal, also demonstrate a good level of model performance (refer to Tables 1 and 2 for further details). However, the model

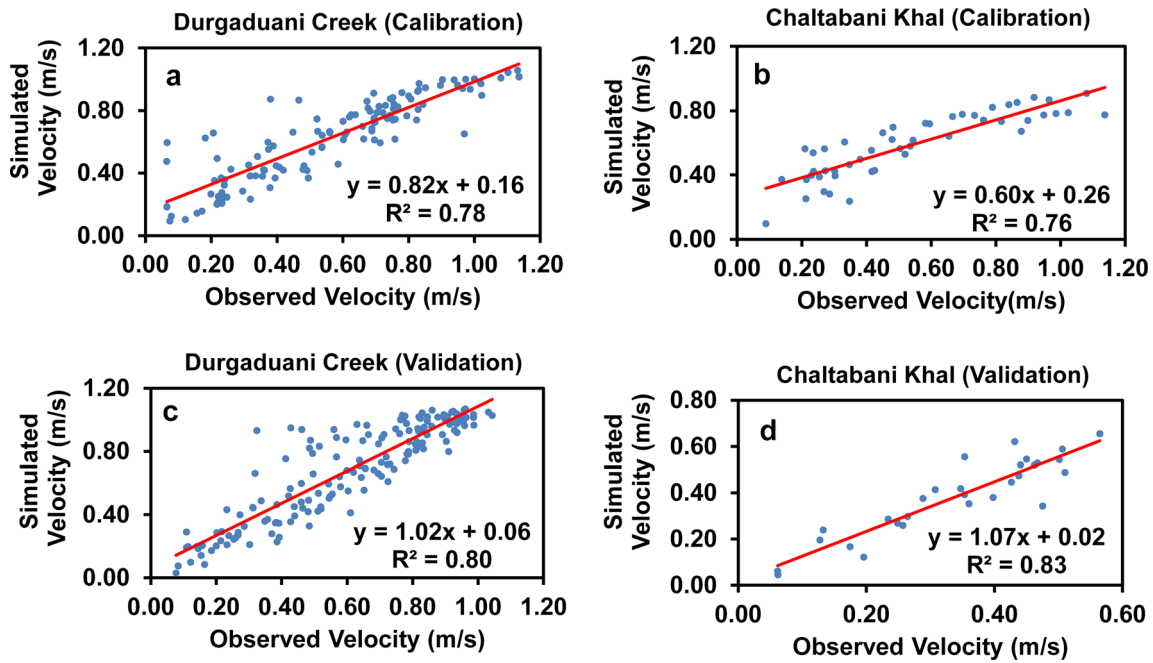


Fig. 4 Correlation between the observed velocity and the simulated velocity during the calibration period (a and b) and the validation period (c and d) at the Durgaduani Creek and Chaltabani Khal

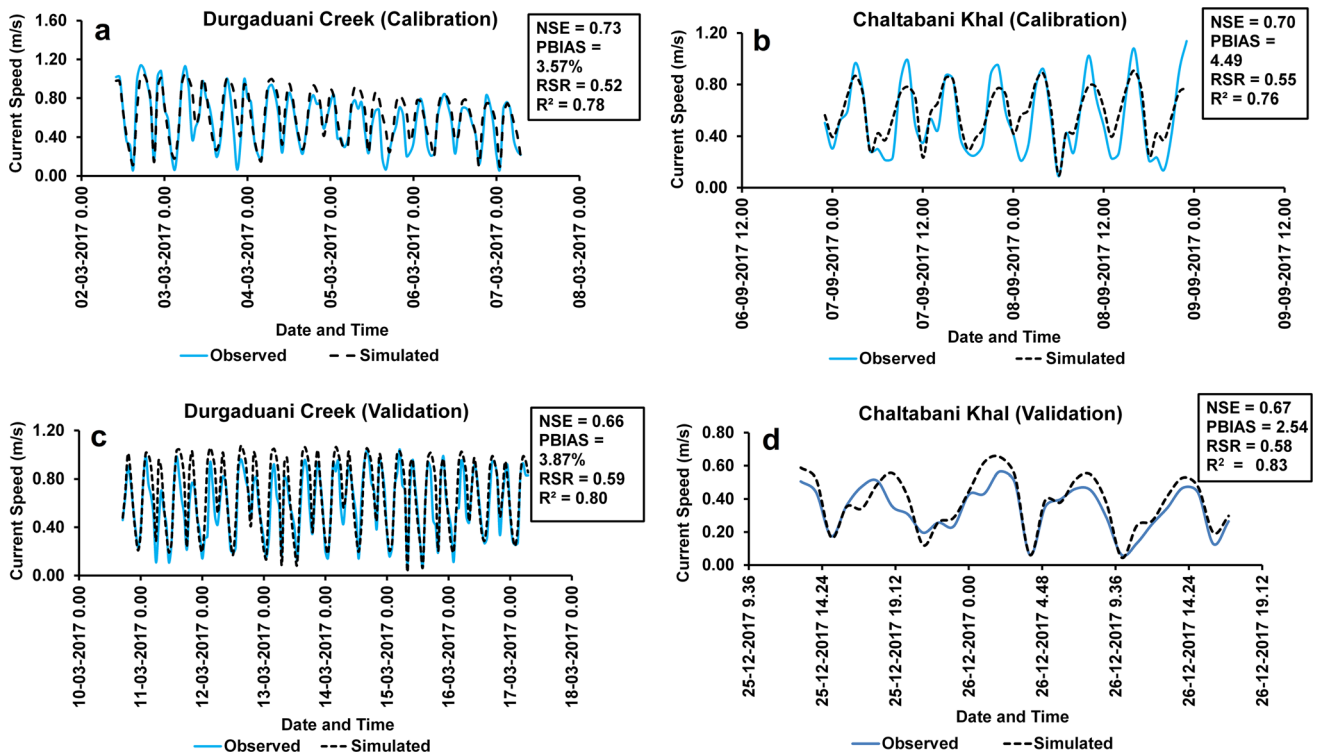


Fig. 5 Calibration at the Durgaduani Creek (a) and the Chaltabani Khal (b); Validation at the Durgaduani Creek (c) and the Chaltabani Khal (d)

performance during the calibration and the validation period ranges from ‘good’ to ‘very good’ with respect to the model performance rating scale (Table 1), and this level

of model accuracy significantly denotes that the MIKE 21 HD model is capable of predicting tidal velocities in this region.

Table 2 Quantitative assessment of model calibration and validation for the Durgaduani Creek and the Chaltabani Khal

| Station | Evaluation of statistics | | | | | | | |
|------------|--------------------------|-------------|-------------|-------------|------------------|------------------|-------------|------------|
| | NSE | | RSR | | PBIAS (%) | | R^2 | |
| | Calibration | Validation | Calibration | Validation | Calibration | Validation | Calibration | Validation |
| Durgaduani | 0.73 (Good) | 0.66 (Good) | 0.52 (Good) | 0.59 (Good) | 3.57 (Very Good) | 3.87 (Very Good) | 0.78 | 0.80 |
| Chaltabani | 0.70 (Good) | 0.67 (Good) | 0.55 (Good) | 0.58 (Good) | 4.49 (Very Good) | 2.54 (Very Good) | 0.76 | 0.83 |

Spatial Variability of Tidal Velocities in the Rivers of the ISD

The average and the maximum velocities during the high tide and low tide (Table 3) were calculated to analyse the spatial distribution of tidal velocities in the rivers of the Sundarbans using the model derived current speeds of March 2017.

The diagrams in Fig. 6 show clear spatial variability of tidal velocities over the Sundarbans. Site F on the Bidyadhari River was characterized by the highest magnitude of tidal velocity during the high tide and low tide (Fig. 6b and c). On the other hand, the tidal velocities in site C on the Thakuran River, site E on the Matla River, and site K on the Harinbhanga River of the Sundarbans remained relatively low.

Temporal Variability of Tidal Velocities in the Rivers of the ISD

To investigate the temporal variability of tidal velocities, the maximum velocities and the average velocities were calculated for the locations of the Durgaduani Creek, Chaltabani Khal, and Gosaba River. Tidal ranges were also

calculated for these locations using the tide level data obtained from WXTide. Figure 7 depicts the monthly variability of tidal velocities along with the tidal ranges at the Durgaduani Creek. It was observed that the highest magnitude of the maximum velocities (Fig. 7a) at the Durgaduani Creek reached up to 1.91 m/s with the highest maximum tidal range of 5.8 m. in April, and the weakest maximum velocity was found to be 1.84 m/s with the tidal range of 5.3 m. in January, although the lowest maximum tidal range was 5.2 m. in February. The maximum velocities for the other months also remained above 1.8 m/s. As the maximum velocities retain their magnitude for a while, they could not be used to analyse a large region; thus, the average velocities (Fig. 7b) were estimated. The variation in average velocities was different from the variation of maximum velocities at the Durgaduani Creek. Figure 7b reveals that the highest average velocity was about 1.15 m/s in March with 4.06 m. average tidal range, whereas the lowest average velocity at the Durgaduani Creek was about 0.92 m/s in August with the lowest tidal range of 3.83 m, though the highest average tidal range was 4.09 m. in December. However, the mean monthly velocities at this location remained near 1 m/s and above for the entire year.

Table 3 Distribution of tidal velocities in the rivers of the ISD

| Site Name (ref. Fig. 6a) | Local name | Channel orientation | Approx. width (m) | Average velocity (m/s) | | Maximum velocity (m/s) | |
|--------------------------|-------------------|---------------------|-------------------|------------------------|-----------|------------------------|-----------|
| | | | | Low tide | High tide | Low tide | High tide |
| A | Muriganga River | North–South | 3000 | 0.52 | 0.56 | 0.77 | 1.00 |
| B | Chaltabani Khal | North–South | 242 | 0.56 | 0.63 | 1.13 | 1.58 |
| C | Thakuran River | East–West | 940 | 0.48 | 0.55 | 0.99 | 1.29 |
| D | Matla River | North–South | 1222 | 0.71 | 0.73 | 1.28 | 1.55 |
| E | Matla River | North–South | 13,000 | 0.49 | 0.53 | 0.94 | 1.11 |
| F | Bidyadhari River | East–West | 190 | 0.95 | 1.21 | 1.71 | 2.46 |
| G | Durgaduani Creek | North–South | 144 | 0.90 | 1.06 | 1.50 | 1.89 |
| H | Matla River | North–South | 312 | 0.75 | 0.80 | 1.10 | 1.42 |
| I | Dutta River | East–West | 150 | 0.53 | 0.68 | 0.74 | 1.25 |
| J | Gosaba River | North–South | 1490 | 0.73 | 0.62 | 1.22 | 1.13 |
| K | Harinbhanga River | North–South | 3400 | 0.57 | 0.49 | 1.00 | 0.91 |

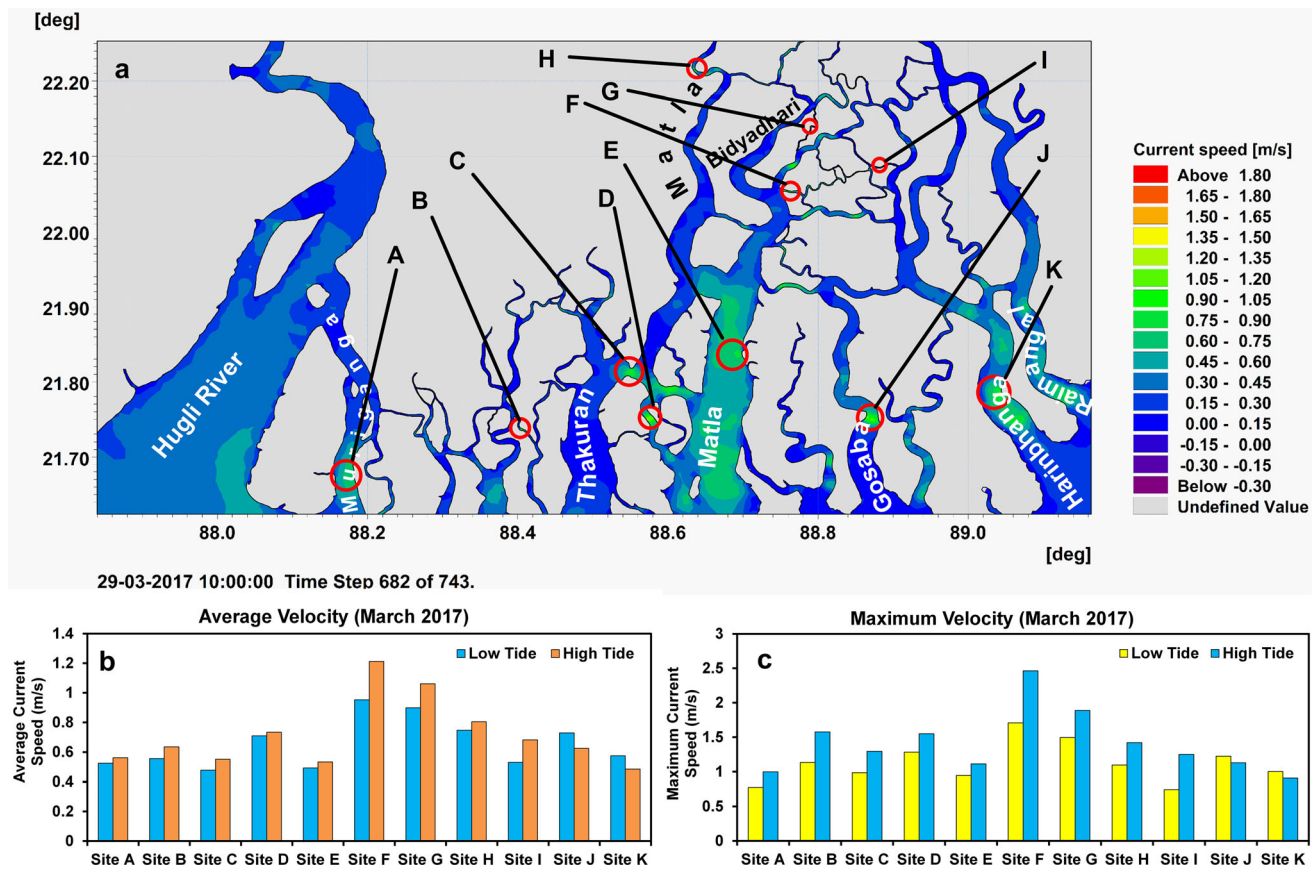


Fig. 6 Spatial variability of tidal velocities in the Rivers of the ISD; variation in **a** high-velocity sites **b** average velocity, **c** maximum velocity during low and high tide

Figure 8 demonstrates that the most significant magnitude of the maximum velocities (Fig. 8a) at the Chaltabani Khal reached up to 1.58 m/s in March along with the maximum tidal range of 3.2 m, and the lowest magnitude of the maximum velocities was found to be 1.17 m/s with the lowest tidal range of 3 m. in August. However, the maximum velocities remained above 1 m/s for all the months of the year. On the other hand, the highest average velocity was 0.59 m/s in March along with the highest average tidal range of 2.26 m, while the lowest average velocity was 0.55 m/s in August along with the lowest tidal range of 2.11 m. (Fig. 8b).

Figure 9 represents the variability of the tidal velocities at the Gosaba River. The greatest magnitude of the maximum velocities (Fig. 9a) at the Gosaba River was 1.22 m/s in March with the maximum tidal range of 3.2 m. The weakest magnitude of the maximum velocities was observed to be 1.19 m/s along with the lowest tidal range of 3 m. in January, followed by July and August. In addition, the highest average velocity of 0.68 m/s (Fig. 9b) was recorded in March along with the highest average tidal range of 2.26 m. in the Gosaba River. In contrast, the lowest average velocity was estimated to be 0.64 m/s along

with the lowest tidal range of 2.11 m. in August. Therefore, the most significant temporal variation of tidal velocities was observed before and after the summer equinox in March (Fig. 9).

Duration of Tidal Velocities in the Rivers of the ISD

In this section, the simulated tidal velocities in different estuarine rivers of the Sundarbans during March 2017 are used to elucidate the time duration of tidal velocities per day. Figure 10 shows a velocity duration curve for the eleven high-velocity sites of the Sundarbans. Each point on the curves demonstrates the number of hours per day for which the corresponding velocity occurred. Site F on the Bidyadhari River exhibited a higher tidal velocities than the other sites. About 53.23% of tidal velocities were more than 1 m/s throughout a day in this site. For other sites, the variation of tidal velocities from 0.5 to 1.0 m/s had a higher time duration throughout a day. However, all the sites are included in the same Fig., so that it can be easily identified which site is the best and most promising for harnessing tidal energy in the future.

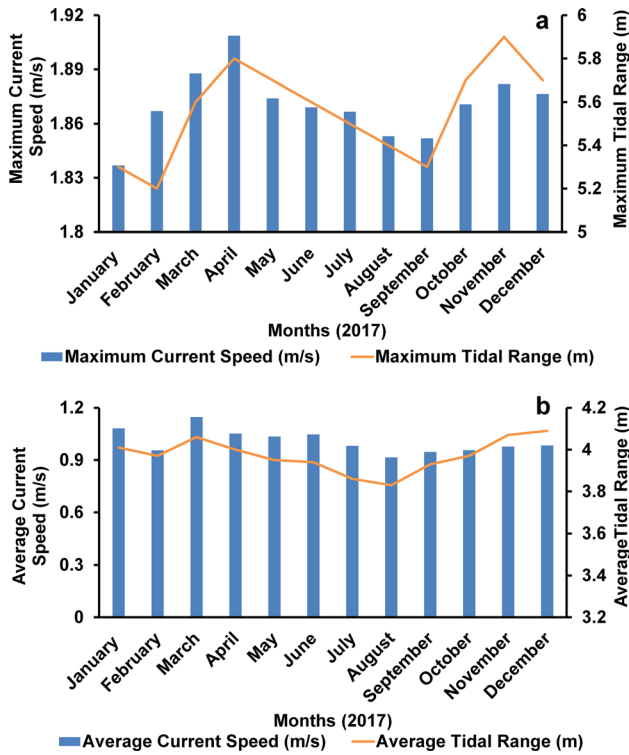


Fig. 7 Monthly Variability of Tidal Velocities along with the Corresponding Tidal Range at Durgaduani Creek, **a** Maximum Velocity and **b** Average Velocity

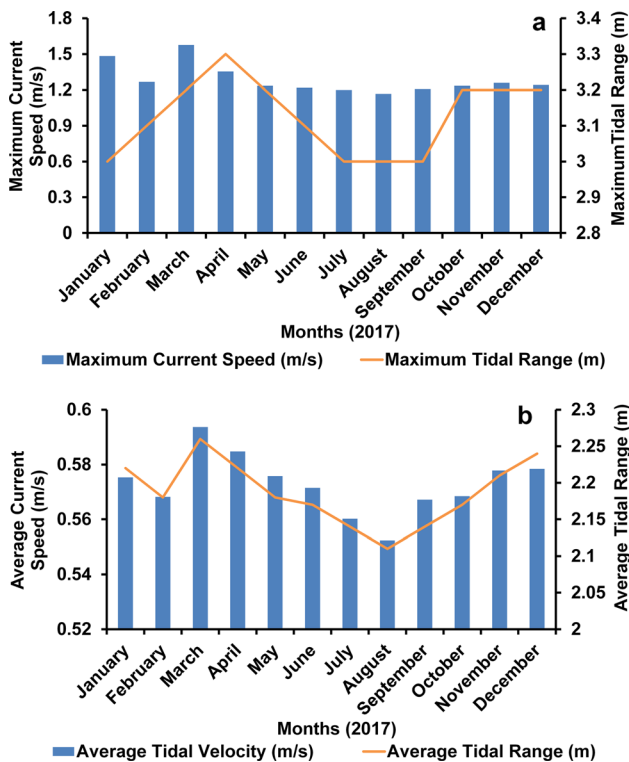


Fig. 8 Monthly variability of tidal velocities along with the corresponding tidal range at Chaltabani Khal, **a** maximum velocity, and **b** average velocity

Identification of Potential Deployment Locations for Tidal Stream Energy in the ISD

Accepting the above calibration and validation process, tidal flow simulation has been carried out for the whole year of 2017 for the whole computational domain shown in Fig. 2. The simulation results indicated 11 high-velocity fields shown in Fig. 6 of which 7 sites shown in Figs. 11, 12 and 13 could be considered as potential high energy sites for any further tidal energy development activities in the Sundarbans.

The maximum spring tide produced a current velocity up to 1.6 m/s for site 1, 1.5 m/s for site 2, 1.3 m/s for site 3, 2.5 m/s for site 4, 1.6 m/s for site 5, 1.9 m/s for site 6 and 1.4 for site 7.

Discussion

The results produced based on model simulations and site measurements suggest that the ISD possesses a significant spatial variability of tidal velocities during the tidal phases. A relatively high velocity appears in the narrower northern region of the estuaries. The wider southern portion of the estuaries exhibits relatively low velocities. The speed of streamflow spatially can vary due to several factors like the

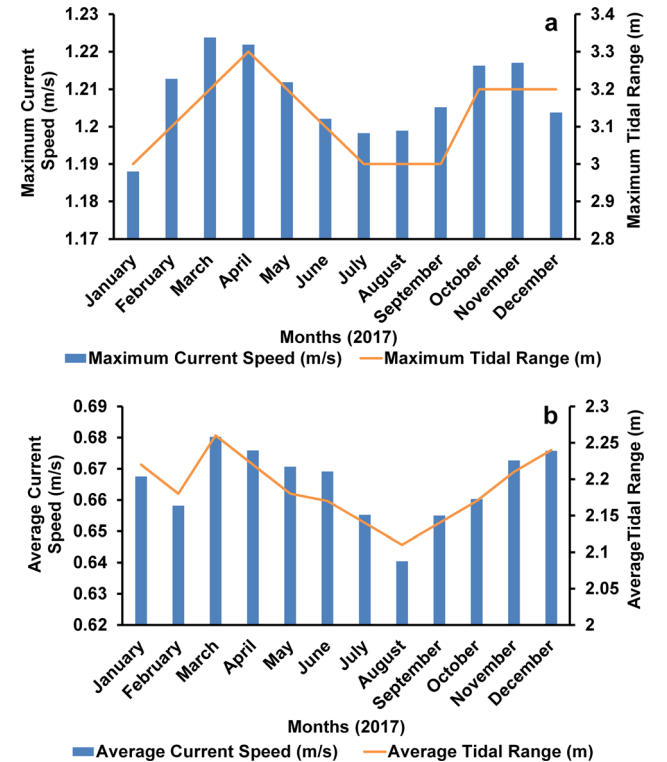


Fig. 9 Monthly variability of tidal velocities along with the corresponding tidal range at Gosaba River, **a** maximum velocity, and **b** average velocity

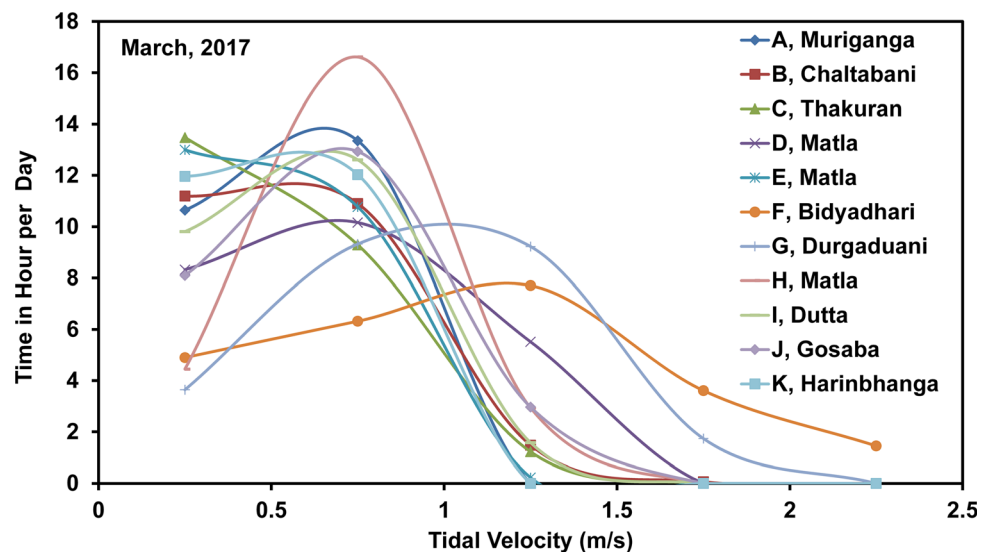
slope of the river bed, depth of water, the hydraulic radius of the channel, bed roughness, amount of water, amount of bedload, the shape of the channel, width of the channel, viscosity of water, cross-sectional area of the channel and the changes of topography [30]. Alternatively, the intensity of tidal velocities may be influenced by the shape of the bays and estuaries, like the variation of magnitudes of tidal velocities in a Funnel-shaped bay [31] as observed in the Sundarbans Estuaries. Moreover, the tidal velocities in the narrow channels of an estuary are relatively stronger than those in the wide channels [32]. This phenomenon is also observed in the present study area, as shown in Table 4.

An inverse relationship is observed between the channel width and the velocity in the rivers and creeks of the Sundarbans Delta region (Table 4 and Fig. 6). Wider channels allow a spread of water mass, which speeds up in the narrower segments on the upstream due to the continuity of the flow [30]. However, other factors, such as depth or slope, may also have some control over the velocities as seen at site D with higher velocities in a wider channel than site B with lower velocities in a narrow but deeper channel. The river bed roughness is another critical factor that regulates the flow velocity of a stream. The mangroves can influence the bed roughness, thereby affecting the current speed in the rivers. Kaiser et al. [33], in the tsunami inundation modelling, healthy mangroves might reduce flow velocities near to 50% due to increased bed roughness. The mangrove swamps in the tidal flood plains store the water in their roots and create a blockage that reduces the flow velocity in the tidal creeks [34]. In this study, the tidal velocities at site J in the Gosaba River and site K in the Harinbhanga River in the Core area of the Mangrove forest were found to be weaker, most likely due to more bed roughness induced by the mangrove trees than in the other parts of the estuaries (Fig. 6 and Table 4). The

flow velocities may also decrease with increasing bed levels and the density of mangrove trees [35]. In the present investigation, it was also revealed that the tidal velocities during the high tidal phase were stronger compared to those in the low tidal phase due to the shorter duration of the flood tide. Stronger flood current and weaker ebb current are implied by a shorter flood tide duration with a compensating longer duration of its fall [17]. Arora et al. [36] stated that the flood tidal velocities in the Hugli Estuary were stronger than the ebb-tidal velocities, and higher bottom stress prevails during the ebb tide compared to the flood tide due to the combined actions of wave and current.

In the present work, the results suggest that the Sundarbans exhibit monthly variations of tidal velocities, which are stronger during the March equinox and weaker around the summer solstice and after, even during the wet monsoon season. During the spring tide, the tide level obtains the highest level at the time of equinoxes, and it falls to the lowest level around the solstices [37]. Pliny the Elder (AD 77) reported in his book ‘Natural History’ that the annual changes of the Sun enhance the tidal effects; the tides are higher at the equinoxes; rather it is higher at the time of autumnal equinox (March) than the vernal equinox (September). It is established in this study that the tidal velocities in March are higher than those in September. Apart from this, it is also indicated by the model results that the tidal velocities also are greater at the period of higher tidal range compared to that during the condition of lower tidal range. The differences in the gradients of horizontal density during these two periods may cause this type of pattern which is consistent with the results [38]. According to El Tawil et al. [39], a linear relationship exists between the current velocity and tidal range. In the present study, few prospective high energy sites were

Fig. 10 Velocity duration curve for the selected sites (Fig. 6a) of the Sundarbans



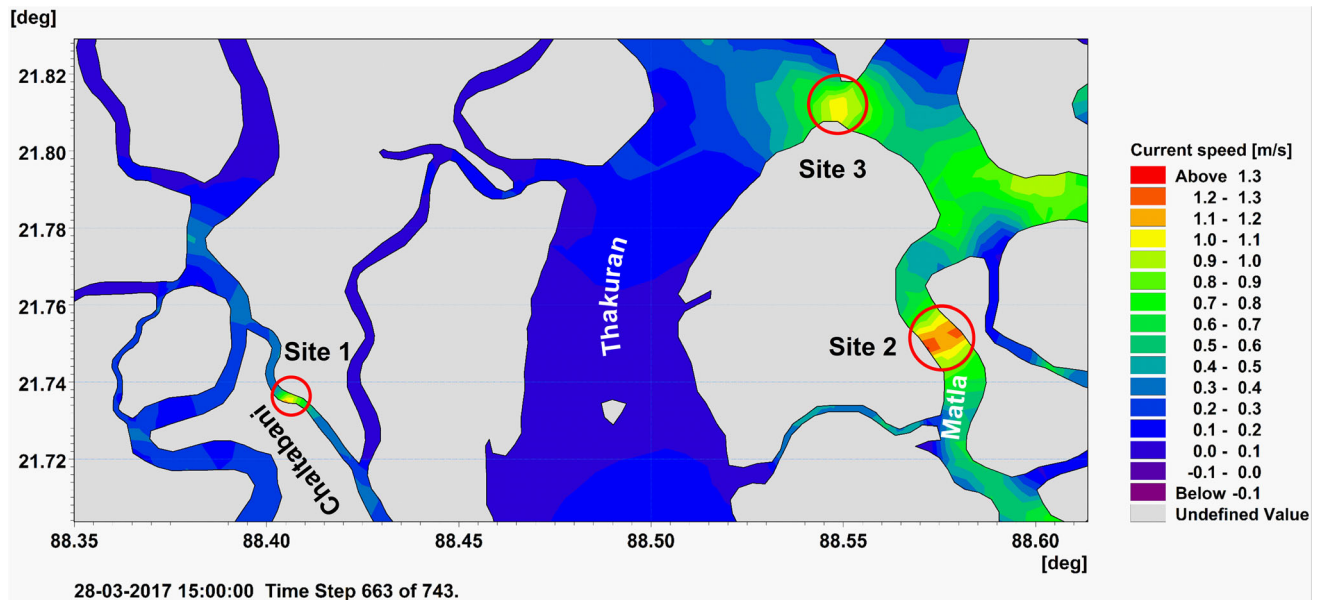


Fig. 11 High energy sites in the Chaltabani Khal and Matla River marked by red circles

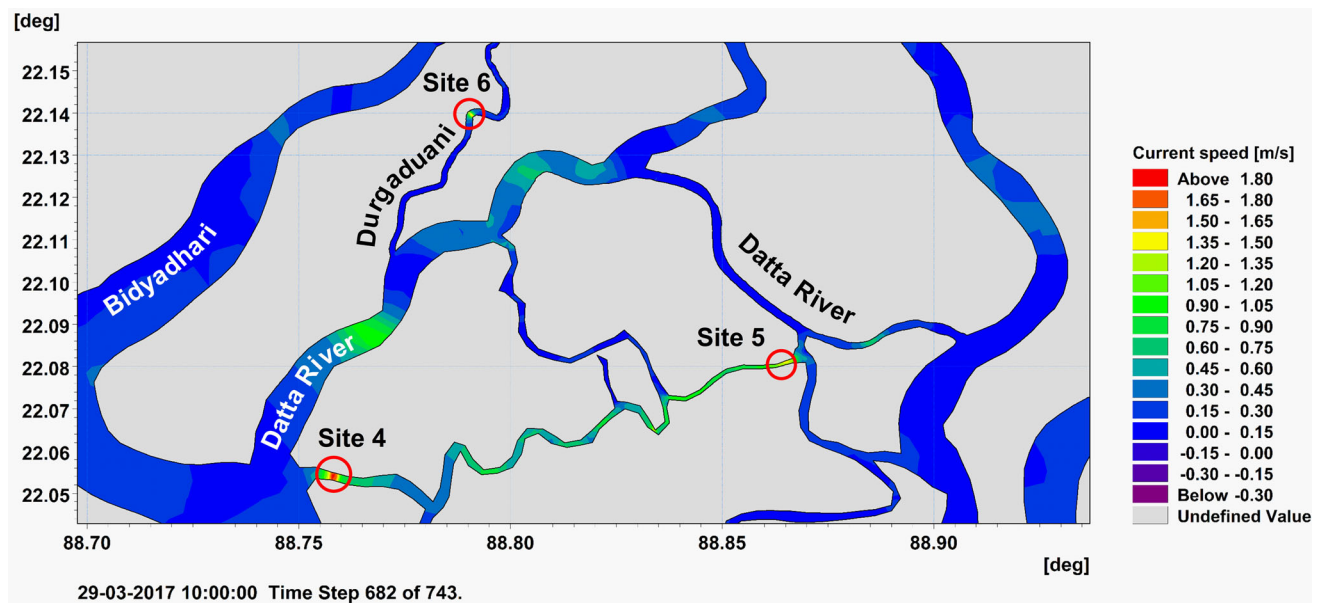


Fig. 12 High energy sites in the Durgaduani Creek and Datta River marked by red circles

considered for harnessing tidal energy. Tidal energy is extremely site-specific and requires a minimum current speed of 1 m/s [40]. The results shown and discussed above are based on limited data (bathymetry and site

measurements) and, although the authors are highly confident about the accuracy of the resulting model parameters, cautions are to be exercised when applying the results to further research or practical use.

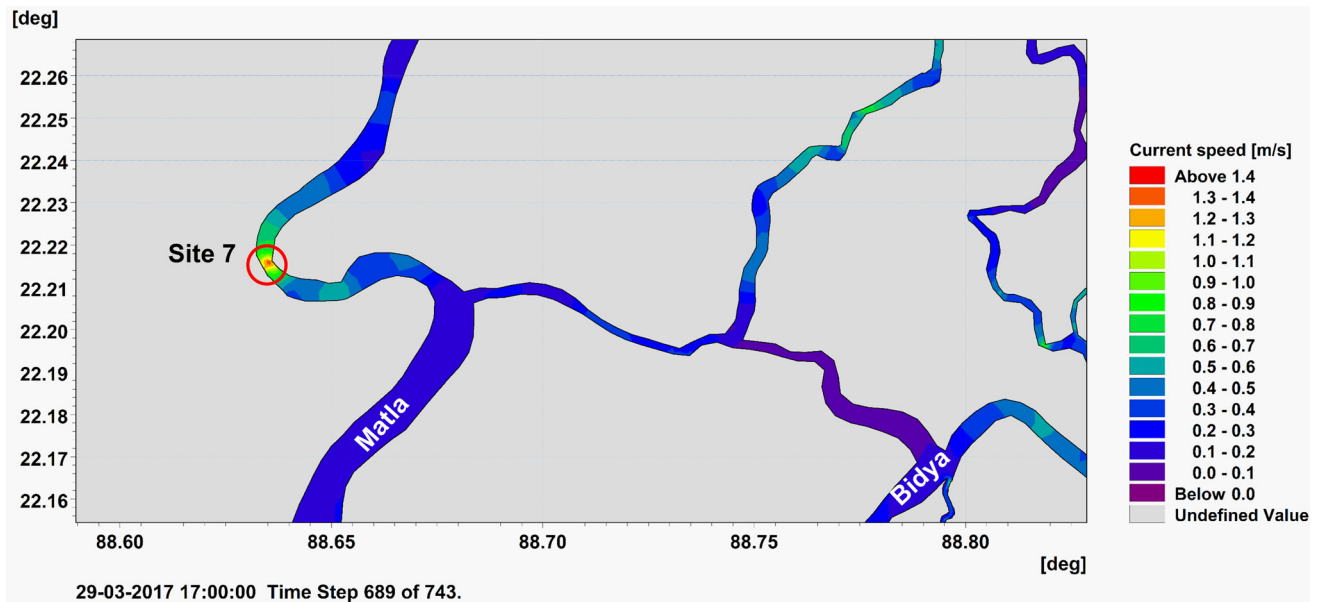


Fig. 13 High energy sites in the Matla River Near Canning marked by red circle

Table 4 Relationship between the channel width and flow velocity in the Sundarbans

| Site name | Local name | Approx. channel width (m) | Mean monthly velocity (m/s) |
|-----------|-------------------|---------------------------|-----------------------------|
| E | Matla River | 13,000 | 0.51 |
| K | Harinbhanga River | 3400 | 0.53 |
| A | Muriganga River | 3000 | 0.54 |
| J | Gosaba River | 1490 | 0.68 |
| D | Matla River | 1222 | 0.72 |
| H | Matla River | 312 | 0.78 |
| F | Bidyadhari River | 190 | 1.09 |

Conclusion

For this research, MIKE 21 HD modelling tool was used to predict tidal velocities in the rivers of the ISD to analyse the Spatio-temporal variability of tidal velocities along and across the estuary. Additionally, to calibrate and validate the model, the tidal velocities systematically measured at two locations using ADCPs were compared with the predicted velocities, which showed a satisfactory match.

The study observed that tidal velocities were comparatively stronger with the higher tidal ranges during the March equinox (March/April) in the period of the dry season, weaker with the lower tidal ranges around the summer solstice (July/August) during the wet season, peaking again during the September equinox. A few high-velocity fields in the Sundarbans Estuaries were identified from the model output. In the narrow channels, the velocities were stronger than those in the wide channels in

the outer estuaries. During March, the maximum velocities exceeding 1 m/s were observed at sites B to J (Fig. 6a) during the high tide phases, while during the low tide, the maximum velocities exceeded 1 m/s at sites B, D, F, G, H, J, and K only (Fig. 6a). Tidal velocities were weaker in the Sundarbans Tiger reserve area than in the outer buffer zones. Observation of higher tidal velocities along the zones of erosion along the island banks and lower velocities along the zones of accretion indicates the dominant control of tidal dynamics on the erosion–accretion process of the delta, particularly in the absence of upstream water and sediment discharge. However, the role of mangroves controlling the erosion deposition process in the Sundarbans delta needs to be explored further. This paper significantly describes the hydrodynamic modelling work for the ISD to identify potential sites for tidal energy. More accurate prediction of the power production from tidal

current speeds at the potential sites will further be achieved in future research.

The GEBCO data are not entirely reliable in the narrow creeks due to its grid size (900 m). More accurate bathymetry data are required for realistic modelling, and therefore in situ bathymetric measurements were used mainly during the present study. Due to limited time and budget, only two stations were selected for calibration and validation. Tidal velocities in other linking rivers, except the Durgaduani and Chaltabani, were not calibrated/validated; hence predicted flow velocities for these rivers should be used with caution. Lack of real-time data was a big challenge to complete the present study, while the inclusion of up-to-date finer bathymetry of the entire study domain can further enhance the reliability of the model results. It is envisaged that extensive measurements of tidal velocity, as well as the water level from several sites of the estuaries, can be undertaken in the future to produce a model more capable of accurate predictions for the entire Sundarbans estuary. Exploring the sites having more than 1 m/s tidal velocity for a longer duration can be another future research direction to produce tidal energy for village electrification in the Sundarbans.

Funding The authors would like to acknowledge *University Grants Commission (UGC)*, India and *DST-UKIERI* which enabled to accomplish the project entitled, ‘Tidal Energy for sustainable village electricity supply in the Indian Sundarban Biosphere’.

Declarations

Conflict of interest The authors have no conflicts of interest to declare.

References

1. A.P. Sharma, K.R. Naskar, Coastal zone vegetation in India with reference to mangroves and need for their conservation. CIFRI (ICAR), Kolkata 9–40 (2010)
2. G.K. Das, *Estuarine Morphodynamics of the Sunderbans* (Springer, Cham, 2015), pp. 1–45
3. J. Seidensticker, M.A. Hai, *The Sundarbans Wildlife Management Plan: Conservation in the Bangladesh Coastal Zone* (IUCN, 1983)
4. L. Rose, P.K. Bhaskaran, Tidal propagation and its non-linear characteristics in the Head Bay of Bengal. *Estuar. Coast. Shelf Sci.* **188**, 181–198 (2017)
5. I.M. Radjawane, F. Riandini, Numerical simulation of cohesive sediment transport in Jakarta Bay. *Int. J. Remote Sens. Earth Sci.* **6**(1), 1240 (2010)
6. T. Dabrowski, M. Hartnett, A. Berry, Modelling hydrodynamics of Irish Sea, in *Computational Fluid and Solid Mechanics 2003*, pp. 877–881 (2003)
7. J.S. Kumar, R. Balaji, Estimation of tidal current energy along the Gulf of Khambhat using three-dimensional numerical modelling. *Int. J. Ocean Clim. Syst.* **8**(1), 10–18 (2017)
8. L.S. Blunden, A.S. Bahaj, Initial evaluation of tidal stream energy resources at Portland Bill, UK. *Renew. Energy* **31**(2), 121–132 (2006)
9. K.K. Balachandran, G.S. Reddy, C. Revichandran, K. Srinivas, P.R. Vijayan, T.J. Thottam, Modelling of tidal hydrodynamics for a tropical ecosystem with implications for pollutant dispersion (Cohin Estuary, Southwest India). *Ocean Dyn.* **58**(3–4), 259–273 (2008)
10. M.T. Babu, P. Vethamony, E. Desa, Modelling tide-driven currents and residual eddies in the Gulf of Kachchh and their seasonal variability: A marine environmental planning perspective. *Ecol. Model.* **184**(2–4), 299–312 (2005)
11. A. Rahman, V. Venugopal, J. Thiebot, On the accuracy of three-dimensional actuator disc approach for a large size turbine in simple channel. *Energies* **11**(8), 2151 (2018)
12. A. Rahman, V. Venugopal, Parametric analysis of three dimensional flow models applied to tidal energy sites in Scotland turbine in simple channel. *Estuar. Coast. Shelf Sci.* **189**, 17–32 (2017)
13. V.S. Kumar, V.R. Babu, M.T. Babu, G. Dhinakaran, G.V. Rajamanickam, Assessment of storm surge disaster potential for the Andaman Islands. *J. Coast. Res.* **24**, 171–177 (2008)
14. T.S. Murty, R.F. Henry, Tides in the Bay of Bengal. *J. Geophys. Res. Oceans* **88**, 6069–6076 (1983)
15. B. Sindhu, A.S. Unnikrishnan, Characteristics of tides in the Bay of Bengal. *Mar. Geod.* **36**(4), 377–407 (2013)
16. S. Bhattacharyya, J. Pethick, K.S. Sarma, Managerial response to sea level rise in the tidal estuaries of the Indian Sundarbans: a geomorphological approach. *Water Policy* **15**, 51–74 (2013)
17. M. Chatterjee, D. Shankar, G.K. Sen, P. Sanyal, D. Sundar, G.S. Michael, A. Chatterjee, P. Amol, D. Mukherjee, K. Suprit, A. Mukherjee, V. Vijith, S. Chatterjee, A. Basu, M. Das, S. Chakraborti, A. Kalla, S.K. Misra, S. Mukhopadhyay, G. Mandal, K. Sarkar, Tidal variations in the Sundarbans estuarine system. *India. J. Earth Syst. Sci.* **122**(4), 899–933 (2013)
18. R. Gayathri, P.L.N. Murty, P.K. Bhaskaran, T.S. Kumar, A numerical study of hypothetical storm surge and coastal inundation for AILA cyclone in the Bay of Bengal. *Environ. Environ. Fluid Mech.* **16**(2), 429–452 (2016)
19. L.M. Bricheno, J. Wolf, S. Islam, Tidal intrusion within a mega delta: An unstructured grid modelling approach. *Estuar. Coast. Shelf Sci.* **182**, 12–26 (2016)
20. C. Antony, A.S. Unnikrishnan, P.L. Woodworth, Evolution of extreme high waters along the east coast of India and at the head of the Bay of Bengal. *Glob. Planet. Change* **140**, 59–67 (2016)
21. L. Rose, P.K. Bhaskaran, Tidal asymmetry and characteristics of tides at the head of the Bay of Bengal. *Q. J. R. Meteorol. Soc.* **143**(708), 2735–2740 (2017)
22. DHI, MIKE21 Flow Model FM User Guide (2014)
23. P.K. Bhaskaran, S. Nayak, S.R. Bonthu, P.L.N. Murty, D. Sen, Performance and validation of a coupled parallel ADCIRC–SWAN model for THANE cyclone in the Bay of Bengal. *Environ. Fluid Mech.* **13**(6), 601–623 (2013)
24. L. Kregting, B. Elsässer, A hydrodynamic modelling framework for Strangford Lough part 1: tidal model. *J. Mar. Sci. Eng.* **2**(1), 46–65 (2014)
25. A.A. Hanipah, Z.R. Guo, E.S. Zahran, Hydrodynamics modelling of a river with mangrove forests. *IET Conf. Publ.* (2018)
26. S. Dasgupta, M. Islam, M. Huq, Z. Khan, M. Hasib, Mangroves as protection from storm surges in Bangladesh. *World Bank Group* (2017). <https://doi.org/10.1596/1813-9450-8251>
27. D.N. Moriasi, J.G. Arnold, M.W. Liew, R.L. Bingner, R.D. Harmel, T.L. Veith, Model evaluation guidelines for systematic quantification of accuracy in watershed simulations. *Trans. ASABE* **50**(3), 885–900 (2007)

28. H. Noh, J. Lee, N. Kang, D. Lee, H.S. Kim, S. Kim, Long-term simulation of daily streamflow using radar rainfall and the SWAT model: a case study of the Gamcheon basin of the Nakdong River, Korea. *Adv. Meteorol.* **2016** (2016)
29. T.W. Chu, A. Shirmohammadi, Evaluation of the SWAT model's hydrology component in the piedmont physiographic region of Maryland. *Trans. Am. Soc. Agric. Eng.* **47**(4), 1057 (2004)
30. M. Morisawa, *Streams; Their Dynamics and Morphology* (McGraw-Hill, New York, 1968), pp. 28–40
31. H.V. Thurman, *Introductory Oceanography*, 7th edn. (Macmillan, New York, 1994), pp. 252–276
32. W.H. Adey, K. Loveland, Estuaries: ecosystem modelling and restoration. *Dyn. Aquaria* **3**, 405–441 (2007)
33. G. Kaiser, L. Scheele, A. Kortenhaus, F. Løvholt, H. Römer, S. Leschka, The influence of land cover roughness on the results of high-resolution tsunami inundation modelling. *Nat. Hazards Earth Syst. Sci.* **11**(9), 2521–2540 (2011)
34. Y. Wu, R.A. Falconer, J. Struve, Mathematical modelling of tidal currents in mangrove forests. *Environ. Model. Softw.* **16**(1), 19–29 (2001)
35. E.M. Horstman, C.M. Dohmen-Janssen, S.J. Hulscher, Flow routing in mangrove forests: a field study in Trang province. Thailand. *Cont. Shelf Res.* **71**, 52–67 (2013)
36. C. Arora, P.K. Bhaskaran, Parameterization of bottom friction under combined wave-tide action in the Hugli estuary. *India. Ocean Eng.* **43**, 43–55 (2012)
37. D.E. Cartwright, *Tides: A Scientific History* (Cambridge University Press, Cambridge, 1999)
38. M.L. Becker, R.A. Luettich Jr., H. Seim, Effects of intratidal and tidal range variability on circulation and salinity structure in the Cape Fear River Estuary, North Carolina. *J. Geophys. Res. Oceans.* **114**(C4), 4972 (2009)
39. T. El Tawil, N. Guillou, J.F. Charpentier, M. Benbouzid, On tidal current velocity vector time series prediction: a comparative study for a French high tidal energy potential site. *J. Mar. Sci. Eng.* **7**(2), 46 (2019)
40. S.C. Bhatia, 13-Tide, wave and ocean energy, in *Advanced Renewable Energy Systems*, 307–333 (2014)

Publisher's Note Springer Nature remains neutral with regard to jurisdictional claims in published maps and institutional affiliations.